Missouri University of Science and Technology
Scholars' Mine

Mechanical and Aerospace Engineering Faculty Research & Creative Works

Mechanical and Aerospace Engineering

01 Jan 1984

Generalized Root-loci Theory For The Static Scherbius Drive

B. Lequesne

Aaron J. Miles
Missouri University of Science and Technology

Follow this and additional works at: https://scholarsmine.mst.edu/mec_aereng_facwork

 Part of the Aerospace Engineering Commons, and the Mechanical Engineering Commons

Recommended Citation

B. Lequesne and A. J. Miles, "Generalized Root-loci Theory For The Static Scherbius Drive," *IEEE Transactions on Power Apparatus and Systems*, vol. PAS thru 103, no. 6, pp. 1304 - 1313, Institute of Electrical and Electronics Engineers, Jan 1984.
The definitive version is available at https://doi.org/10.1109/TPAS.1984.318464

This Article - Journal is brought to you for free and open access by Scholars' Mine. It has been accepted for inclusion in Mechanical and Aerospace Engineering Faculty Research & Creative Works by an authorized administrator of Scholars' Mine. This work is protected by U. S. Copyright Law. Unauthorized use including reproduction for redistribution requires the permission of the copyright holder. For more information, please contact scholarsmine@mst.edu.

GENERALIZED ROOT-LOCI THEORY FOR THE STATIC SCHERBIUS DRIVE

B. Lequesne, A. R. Miles, Member, IEEE

University of Missouri
Rolla, Missouri 65401

Abstract - Generalized root-loci techniques, developed in the mid 70's for squirrel cage motors, have been extended in the static Scherbius configuration to wound rotor, slip energy, recovery systems. This arrangement is now applied to large power drives in the 0.5 to 50 MW range. In this paper, general results applicable to all machines are presented for the open-loop control scheme, but only the subsynchronous mode of operation in which a voltage source type inverter is used is addressed.

INTRODUCTION

The static Scherbius drive is well known for its adjustable speed characteristics and performance efficiency. A recent account [1] of these favorable characteristics and the moderate cost of the drive suggest that it is still very much favored for very large drives on the order of 50 MW.

The drive has received the attention of several researchers. Lavi and Polge [2] analyzed both the steady state and transient state by using a voltage source inverter, but their closed form model does not take into account the effects of motor leakage inductance. However, they later used an iterative method to assess the leakage. For the transient state, they presented only a reduced (second) order model. Miljanic [3] introduced a through-pass inverter to improve the power factor, and Shepherd and Stanway [4] recommended the stator feedback method for the same purpose but at the cost of less efficiency. Bird and Mehta [5] addressed the matter of regeneration, and Smith [6] discussed the use of a cycloconverter instead of an inverter from the standpoint of steady state analysis only and reported that the experimental dynamic response was satisfactory. Pavlov et al. [7] developed a hybrid drive in which the subsynchronous Scherbius was one mode of operation. They did include the motor leakage reactances in their steady state analysis but did not make a transient analysis. A very complete analysis of a closed-loop system was made by Giannakopoulos and Galanos [8], who did not linearize but numerically integrated the differential equations. They also used the fifth order motor model and accounted for the different circuit topology introduced by thyristor switching. Because their technique is numerical, it is disadvantageous because no general conclusions can be drawn with it immediately. Mittle and his coworkers [9,10] used the fifth order model for transient analyses but neglected the effect of leakage inductances. Tsuchiya [11], as did Smith [6] used a cycloconverter on the low order model of the system but updated his analysis by introducing a microprocessor. Franz and Meyer [12] made an analysis that is similar to the one made by Giannakopoulos and Galanos [8], and Smith [13] substituted a current source type inverter for the voltage source type used previously.

In the present paper, the operation of the Scherbius drive with a voltage source type of inverter is examined in both the steady state and dynamic state with emphasis being placed on the latter. Specifically, the so-called generalized root-loci theory [14-17] is extended to this type of drive. To date, only the open-loop operation has been considered, but work is now being conducted on closed-loop feedback situations. The full fifth order model is used in the analysis, and account is taken of motor leakage reactances. The switching of the power electronics is considered to be ideal.

SYSTEM CONFIGURATION

The system that is being studied is presented in Figure 1.

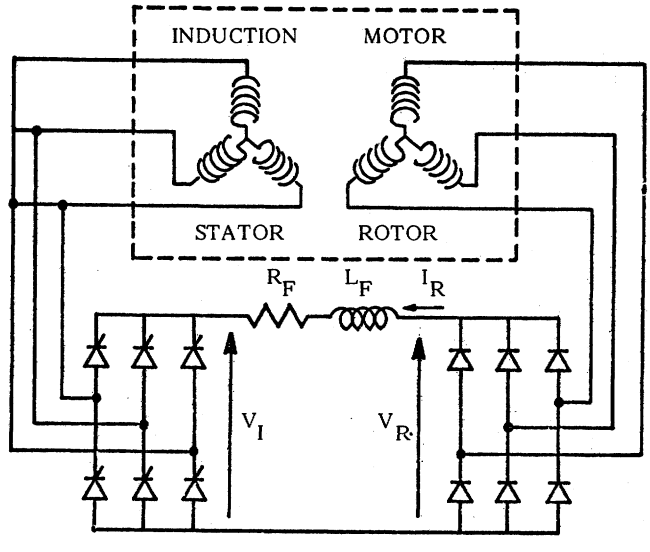

Fig. 1. System Configuration

The excess energy in the rotor can be brought back into the stator through the rectifier-inverter loop. The amount of that energy is controlled by the firing-angle of the thyristors of the inverter. In the process, the rotor voltage is determined. The intermediate dc voltage must be filtered in order to limit the harmonic content in the rotor as much as possible. This is the role of the inductance, L_F. The resistance, R_F, models all the Joule losses in the different elements, particularly the inductance.

The machine model employed in the present study is a conventional, idealized machine with power invariant, two-phase variables. The equations are condensed by writing them in a complex form, and the small signal equations and transfer functions can be derived in the same complex form. The equations are expressed in a synchronous reference frame.

In this simplified approach, the influence of the harmonics is neglected. Even though the rectifier-inverter, by its nature, induces some harmonics into the rotor, it has been shown that they produce relatively small torques [2]. Also, the diodes and thyristors are assumed to be ideal and do not interfere with the dynamics of the system.

83 SM 480-1 A paper recommended and approved by the IEEE Rotating Machinery Committee of the IEEE Power Engineering Society for presentation at the IEEE/PES 1983 Summer Meeting, Los Angeles, California, July 17-22, 1983. Manuscript submitted November 15, 1982; made available for printing May 13, 1983.

0018-9510/84/0600-1304$01.00 © 1984 IEEE

Authorized licensed use limited to: Missouri University of Science and Technology. Downloaded on July 17,2023 at 13:33:30 UTC from IEEE Xplore. Restrictions apply.

STEADY-STATE

The induction machine is represented in its complex form by the three equations noted below in which by convention the real part represents the direct axis and the imaginary part the quadratic axis. In the equations, a complex entity is denoted by a line over its symbol, an asterix indicates a complex conjugate, and the subscript zero signifies a steady-state value. The symbols are defined in Appendix A.

$$\bar{v}_{s_o} = \bar{Z}_{s_o}\,\bar{i}_{s_o} + \bar{Z}_{m_o}\,\bar{i}_{r_o} \tag{1}$$

$$\bar{v}_{r_o} = \bar{Z}_{d_o}\,\bar{i}_{s_o} + \bar{Z}_{r_o}\,\bar{i}_{r_o} \tag{2}$$

$$T = nM\ \mathrm{Im}\,(\bar{i}_{s_o}\,\bar{i}_{r_o}^{*}) = (J/n)p\omega_{r_o} + T_L \tag{3}$$

Because the choice of the axes is arbitrary, the direct axis can be placed alongside the rotor voltage, i.e., v_{ro_q} is equal to zero, and $\bar{v}_{r_o}$ is equal to a real number.

The rectifier can only pump energy from the three windings of the rotor, and there is no periodic exchange of energy between the two sides of the rectifier. Therefore, the rectifier is only a passive element, such as a resistance is [2]. This principle is translated by stating that the rotor voltage (the voltage across the rotor windings) and rotor current must be in phase (such as they would be across a resistance). This means, in view of the choice of axes, that i_{ro_q} is equal to zero, and $\bar{i}_{r_o}$ is a real number.

The rectifier-inverter is represented by the following equations across each bridge:

$$V_I = \frac{3\sqrt{2}}{\pi}\,|\bar{v}_{so}|\cos\gamma \tag{4}$$

and

$$V_R = \frac{3\sqrt{2}}{\pi}\,v_{r_o}. \tag{5}$$

In these equations, $|\bar{v}_s|$ is the modulus of the complex number $\bar{v}_s$, and γ the firing angle of the thyristors. The energy conservation principle yields

$$V_R I_R = -v_{r_o}\,i_{r_o}. \tag{6}$$

Finally, on the dc side

$$V_I = V_R - R_F\,I_R. \tag{7}$$

Because the harmonics are neglected, only the direct component is considered, thus the ripple is supposed to be completely smoothed by L_F, which is not included in Eq. (7) but is used in the dynamics.

Equations (4) through (7) can be summarized as follows:

$$|\bar{v}_{so}|\cos\gamma = v_{r_o} + \frac{\pi^2}{18}\,R_F\,i_{r_o}. \tag{8}$$

Because v_{r_o} can be written as

$$v_{r_o} = \bar{Z}_{r_o}\,i_{r_o} + \bar{Z}_{d_o}\,\bar{i}_{s_o} \tag{2}$$

and because

$$\bar{Z}_{r_o} = R_r + jL_r\omega_{s_o} \tag{9}$$

it should be noted that R_F (with its coefficient $\pi^2/18$) is merely added to the rotor resistance, R_r.

This development must be completed by some reflexions about the signs. For example, Eq. (2) can be divided into two equations on the direct (Eq. (10)) and quadratic (Eq. (11)) axes.

$$v_{r_{o_d}} = v_{r_o} = R_r\,i_{r_o} - M\omega_{s_o}\,i_{s_{o_q}} \tag{10}$$

$$v_{r_{o_q}} = 0 = L_r\omega_{s_o}\,i_{r_o} + M\omega_{s_o}\,i_{s_{o_d}} \tag{11}$$

When energy leaves the rotor, v_{ro} is the voltage across it, and Eq. (10), with the rotor winding resistance R_r, implies that $v_{ro}i_{ro}$ is less than zero. The directions of V_R and I_R shown in Figure 1 imply that $V_R I_R$ is greater than zero, thus justifying the minus sign in Eq. (6). Because energy flows back to the stator, the firing angle, γ, must be greater than 90 degrees, and V_I, V_R, and then v_{ro} are negative as implied in Eqs. (4), (5), and (8). In conclusion, v_{ro} is negative, and i_{ro} is, therefore positive. In fact, this sign system corresponds merely to the choice of a direction for the direct axis, and v_{ro} and i_{ro} can be written as

$$v_{ro} = |v_{ro}|\,e^{j\pi} = -|v_{ro}| < 0 \tag{12}$$

and

$$i_{r_o} = |i_{r_o}|\,e^{j0} = +|i_{ro}| > 0. \tag{13}$$

These equations are all that one needs to solve the steady-state problem for a given firing-angle, γ, and they can be used in the following manner: $|v_{so}|$ can be computed with Eq. (1) and compared with Eq. (8) in which v_{ro} can be replaced by Eq. (10). This leads to an equation, which involves only the currents, that can ultimately be expressed in terms of the ratio $S = i_{soq}/i_{ro}$ (q-component of stator current over rotor current) as follows:

$$\left[(R_s^2 + L_s^2\omega_o^2)\,S^2 + 2MR_s\,\omega_o\,S + \left(\frac{R_s^2 L_r^2}{M^2} + (L_r L_s - M^2)\omega_o^2\right)\right] x\cos^2\gamma = \left[M\omega_{so}\,S - \left(R_r + \frac{\pi^2}{18}\,R_F\right)\right]^2. \tag{14}$$

The ratio S, as expressed in Eq. (14), is linked to the operating point through the rotor frequency, ω_{so}, only. It will be of interest later on.

After Eqs. (3) and (13), the torque can be expressed in a real form, as follows:

$$T_o = nM\,i_{ro}\,i_{soq}. \tag{15}$$

Because the torque is positive, it is clear that S must be positive, thus one of the two solutions of Eq. (14) can be selected without question.

Authorized licensed use limited to: Missouri University of Science and Technology. Downloaded on July 17,2023 at 13:33:30 UTC from IEEE Xplore. Restrictions apply.

The torque-slip characteristics for different γ are shown in Figure 2.

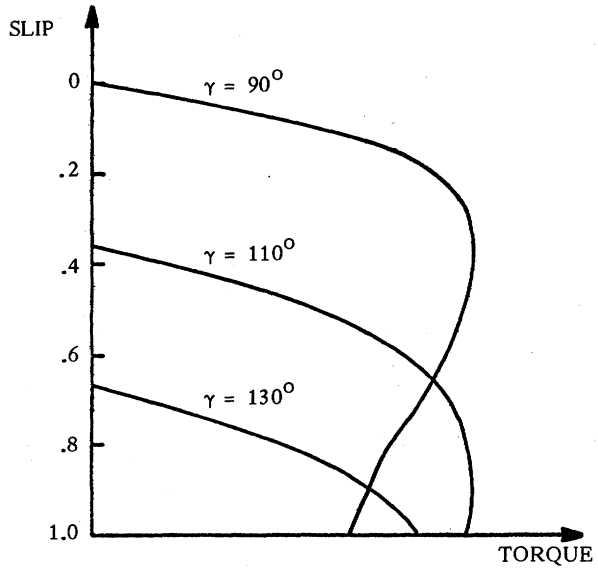

Fig. 2. Torque-slip characteristics for different γ.

The value of slip for which the torque is zero can be found as follows: From Eq. (15), the torque is zero when i_{ro} is zero ($i_{soq} = 0$ does not yield a solution). The use of this idea in the steady-state equations yields

$$s = -\frac{\sqrt{R_s^2 + L_s^2\omega_o^2}}{M\omega_o}\cos\gamma \approx -\frac{L_s}{M}\cos\gamma \approx -\cos\gamma \qquad (16)$$

DYNAMICS

Block Diagram

The transfer function of main interest links a variation of torque to a variation in the rotor speed, ω_r. In the case of the induction motor, this means a fictitious closed-loop system, as represented in Fig. 3a. Both stator voltage and network frequency are kept constant, but the rotor voltage may vary. Figure 3b shows the specific link created by the rectifier-inverter, which associates variations of rotor voltage to variations of rotor current, which in turn can be linked through the general equations of the machine to ω_r. The study of the dynamics is completed by first finding the overall open-loop transfer function, $G_r' = -(\Delta T/\Delta\omega_r)$, and then associating it with the inertia transfer function, $G_j = 1/[(J/n)p]$, in the closed loop shown in Figure 3b.

The small variations technique applied to the general equations of the machine, Eqs. (1) and (2), yield for a constant supply frequency, ω,

$$\Delta\bar{v}_s = Z_s\Delta\bar{i}_s + Z_m\Delta\bar{i}_r \qquad (17)$$

and

$$\Delta\bar{v}_r = Z_d\Delta\bar{i}_s + Z_r\Delta\bar{i}_r - j\Phi_{r_o}\Delta\omega_r \qquad (18)$$

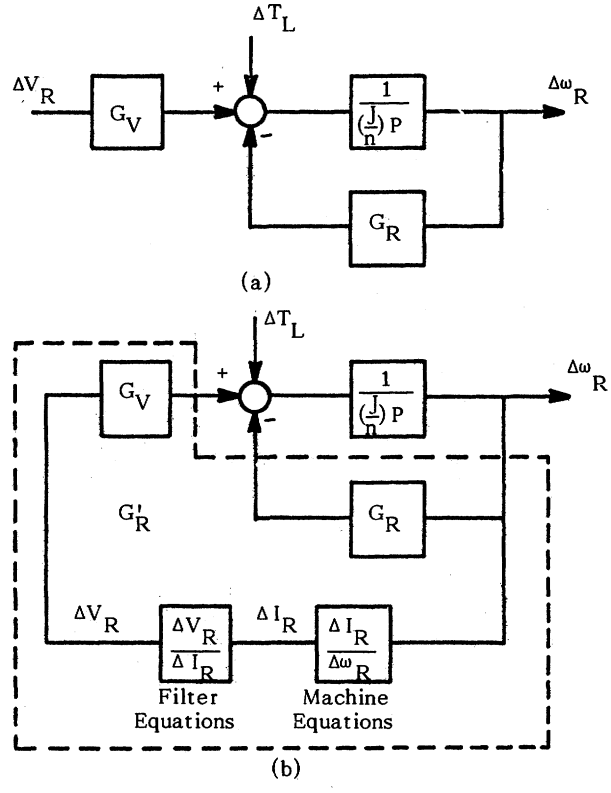

Fig. 3. Open-loop transfer function, G_r'.

in which

$$\Phi_{r_o} = L_r\bar{i}_{r_o} + M\bar{i}_{s_o} = L_r i_{r_o} + M\bar{i}_{s_{o_d}} + jMi_{s_{o_q}}, \qquad (19)$$

and Z_s, Z_m, Z_d, and Z_r are operational impedances (see Appendix A). Because of Eq. (11), Φ_{ro} can be simplified to

$$\Phi_{ro} = jMi_{s_{o_q}}. \qquad (20)$$

Also,

$$\Delta T = nM\,\mathrm{Im}\,(\bar{i}_{so}\,\Delta\bar{i}_r^* + \bar{i}_{ro}^*\,\Delta\bar{i}_s), \qquad (21)$$

hence,

$$\Delta T = nM\,\mathrm{Im}\,(i_{ro}\,\Delta\bar{i}_s - \bar{i}_{so}^*\,\Delta\bar{i}_r). \qquad (22)$$

The stator supplies a constant voltage, implying that $|\Delta\bar{v}_s| = 0$. If the axes are allowed to swing along with $\bar{v}_s$, one can assume that the phase of $\bar{v}_s$ remains constant. Altogether,

$$\Delta\bar{v}_s = 0 \qquad (23)$$

Equation (23) enables one to express $\Delta\bar{i}_s$ in Eq. (17). Then

$$\Delta\bar{v}_r = \frac{\xi}{Z_s}\Delta\bar{i}_r + Mi_{s_{o_q}}\Delta\omega_r \qquad (24)$$

Authorized licensed use limited to: Missouri University of Science and Technology. Downloaded on July 17,2023 at 13:33:30 UTC from IEEE Xplore. Restrictions apply.

and

$$\Delta T = -nM\ \mathrm{Im}\left(\frac{Z_m \bar{i}_{ro} + Z_s \bar{i}^*_{so}}{Z_s}\ \Delta\bar{i}_r\right) \tag{25}$$

in which $\xi = Z_s Z_r - Z_m Z_d$.

This equation system can be completed by taking the rectifier-inverter loop into consideration. During the variations, the rectifier always remains a passive load. Therefore, $\bar{v}_r \bar{i}_r^*$ is real, which means that $\bar{v}_r$ and $\bar{i}_r$ stay on the same axis and have the same phase shift, $\Delta\theta$, from their respective steady-state values. Hence, Eqs. (12) and (13) become

$$\Delta\bar{v}_r = -\Delta|v_r| + j\, v_{ro}\Delta\theta \tag{26}$$

and

$$\Delta\bar{i}_r = \Delta|i_r| + j\, i_{ro}\,\Delta\theta. \tag{27}$$

To the rectifier-inverter loop, Eqs. (4) through (7), one can also apply small variations as follows:

$$\Delta|\bar{v}_s| = 0 \Rightarrow \Delta V_I = 0, \tag{28}$$

$$\Delta V_R = \frac{3\sqrt{2}}{\pi}\ \Delta|\bar{v}_r|, \tag{29}$$

$$\Delta V_I = 0 = \Delta V_R - (R_F + L_F p)\,\Delta I_R, \tag{30}$$

and

$$\Delta(v_r i_r) = -\Delta(V_R I_R). \tag{31}$$

They yield

$$\Delta|\bar{v}_r| = X_F\,\Delta|\bar{i}_r| \tag{32}$$

in which

$$X_F = \frac{\pi^2}{18}\ (R_F + L_F p). \tag{33}$$

Equations (32), (26), (27), and (24) give

$$\frac{\Delta\bar{i}_r}{\Delta\omega_r} = -Mi_{soq}\ \frac{\left(v_{ro} - \left(\frac{\xi}{Z_s}\right)^* i_{ro}\right)}{\left[X_F + \mathrm{Re}\left(\frac{\xi}{Z_s}\right)\right]\left[v_{ro} - i_{ro}\,\mathrm{Re}\left(\frac{\xi}{Z_s}\right)\right] - i_{ro}\left[\mathrm{Im}\left(\frac{\xi}{Z_s}\right)\right]^2} \tag{34}$$

$G'_r = -(\Delta T/\Delta\omega_r)$ can be readily deduced from Eqs. (25) and (34). After some rearrangement,

$$G'_r = -\frac{nM^2 i_{soq}\ \mathrm{Im}\left[(Z_s i_{so}^* + Z_m i_{ro})(Z_s^* v_{ro} - \xi^* i_{ro})\right]}{v_{ro}X_F|Z_s|^2 + (v_{ro} - X_F i_{ro})\mathrm{Re}(\xi Z_s^*) - i_{ro}|\xi|^2} \tag{35}$$

An analysis of Eq. (34) shows that the rotor resistance, R_r, and the filter resistance, R_F, (multiplied by the coefficient $\pi^2/18$), whenever they appear, are added together, thus confirming the idea that they play an identical role with respect to the machine in the steady state as well as the dynamic state.

It is interesting to group the steady-state terms as much as possible. By using Eq. (10) for v_{ro} and the ratio, S, as defined and expressed in Eq. (14), it is possible to extract the steady-state torque, as expressed in Eq. (15), from Eq. (35) as follows:

$$G'_r = -T_o\ \frac{\mathrm{Im}\left[(MZ_m - L_r Z_s - jMZ_s S)(R_r Z_s^* - \xi^* - MZ_s^* \omega_{so} S)\right]}{X_F|Z_s|^2(R_r - M\omega_{so}S) + (R_r - M\omega_{so}S - X_F)\mathrm{Re}(\xi Z_s^*) - |\xi|^2}. \tag{36}$$

Because, as demonstrated by Eq. (14), S is an explicit function of the slip only, the above expression separates T_o on the one hand and machine parameters and slip on the other hand.

Fictitious Closed-Loop Transfer Function

The open loop transfer function, G'_r, must be associated with the inertia transfer function, G_j (Fig. 3), to form the following "fictitious" closed-loop transfer function, $G_j[1+G_jG'_r]$, in which

$$G_j = \frac{1}{\frac{J}{n}p}\ . \tag{37}$$

The behavior of the machine can be determined by computing the roots of the characteristic equation

$$1 + G_j G'_r = 0 \tag{38}$$

with G_j expressed in Eq. (37) and G'_r in Eq. (36). This constitutes a fifth-order polynomial equation in p. It can be fed in this form to the computer to yield the roots. However, in this form, only the usual parameters of the machine appear, and it may seem desirable to reduce their number to simplify the analysis.

Normalized Coefficients

Work has been conducted by Novotny and his coworkers [14-16] to achieve this goal, and a set of nondimensional parameters has been devised for a short-circuited rotor (Table 1).

This set of parameters will be modified and augmented in such a way that it will encompass the specific terms introduced by the rectifier-inverter loop, namely the firing-angle, γ, and the filter parameters, R_F and L_F.

As far as R_F is concerned, it is clear that its role is analogous to that of R_r, and the two are always added to each other. It seems, therefore, convenient to modify the definition of α_r (and hence of α) to take this new factor into account as follows:

$$\alpha_r = (R_r + \frac{\pi^2}{18}R_F)/\sigma L_r\ . \tag{39}$$

Authorized licensed use limited to: Missouri University of Science and Technology. Downloaded on July 17,2023 at 13:33:30 UTC from IEEE Xplore. Restrictions apply.

Table 1

Nondimensional Parameters

$\alpha = \dfrac{\alpha_s}{\alpha_r}$	
with $\alpha_r = \dfrac{1}{T'_r} = \dfrac{R_r}{\sigma L_r}$	Inverses of rotor and stator transient time constants
$\alpha_s = \dfrac{1}{T'_s} = \dfrac{R_s}{\sigma L_s}$	
$\sigma = 1 - M^2/(L_s L_r)$	Leakage parameter
$\tilde{\omega} = \omega/\alpha_r$	Normalized frequencies
$\tilde{\omega}_s = \omega_s/\alpha_r$	
$\lambda = p/\alpha_r$	Normalized eigenvalue

The case of L_F is not as simple, because it intervenes in a different manner in the steady state and the dynamics; however, it is always associated with L_r (rotor inductance), and it is convenient to define the following dimensionless parameter:

$$L_{DL} = \frac{\pi^2}{18}\frac{L_F}{\sigma L_r} . \tag{40}$$

It is possible at this point to express each parameter of the machine in terms of L_r and L_s, with the help of one or another of the above parameters. The function G_I^+ can be split into its numerator and denominator as follows:

Numerator:

$$\left(\frac{\sigma^2 L_r^2 L_s^2 \alpha_r^3 T_o}{\tilde{\omega}_{so}}\right) x \left[\left(\frac{MS\tilde{\omega}_{so}}{\sigma L_r}\right)^2 \left(\lambda^2+2\sigma\alpha\lambda+\sigma^2\alpha^2+\tilde{\omega}_o^2\right) + \left(\frac{MS\tilde{\omega}_{so}}{\sigma L_r}\right)\left(\lambda^3+\lambda^2\alpha(1+\sigma)+\lambda(\sigma\alpha^2+\tilde{\omega}_o^2)\right) - \tilde{\omega}_{so}^2(\lambda^2+2\alpha\lambda+\alpha^2+\tilde{\omega}_o^2)\right] \tag{41}$$

Denominator:

$$(\sigma^2 L_r^2 L_s^2 \alpha_r^4) x \left[L_{DL}\left(\frac{MS\tilde{\omega}_{so}}{\sigma L_r}\right)\left(\lambda^3+2\sigma\alpha\lambda^2+(\sigma^2\alpha^2+\tilde{\omega}_o^2)\lambda\right) + \left(\frac{MS\tilde{\omega}_{so}}{\sigma L_r}\right)\left(\lambda^3+\lambda^2(1+\alpha+\sigma\alpha)+\lambda(2\sigma\alpha+\sigma\alpha^2+\tilde{\omega}_o^2) + \sigma^2\alpha^2+(1-\sigma)\alpha\tilde{\omega}_o\tilde{\omega}_{so}+\tilde{\omega}_o^2\right) + L_{DL}(\lambda^4+\lambda^3\alpha(1+\sigma)+\lambda^2(\sigma\alpha^2+\tilde{\omega}_o^2)+\lambda(1-\sigma)\alpha\tilde{\omega}_o\tilde{\omega}_{so}) + \lambda^4+\lambda^3(1+2\alpha)+\lambda^2(\alpha+\alpha^2+\sigma\alpha+\tilde{\omega}_o^2+\tilde{\omega}_{so}^2) + \lambda(\sigma\alpha^2+\tilde{\omega}_o^2+2\alpha\tilde{\omega}_{so}^2) + (1-\sigma)\alpha\tilde{\omega}_o\tilde{\omega}_{so}+\tilde{\omega}_{so}^2(\alpha^2+\tilde{\omega}_o^2)\right] . \tag{42}$$

These equations include terms in S, as defined in Eq. (14), which always appears in the following form:

$$U = \frac{M\tilde{\omega}_{so}}{\sigma L_r} S. \tag{43}$$

Equation (14) can also be expressed with the dimensionless parameters. Moreover, if the change of variables, Eq. (43), is applied to Eq. (14), one obtains

$$\left[\frac{\sigma^2\alpha^2+\tilde{\omega}_o^2}{\tilde{\omega}_{so}^2}U^2+2\alpha\frac{\tilde{\omega}_o}{\tilde{\omega}_{so}}U+\alpha^2+\tilde{\omega}_o^2\right]\left(\frac{L_s}{M}\cos\gamma\right)^2-(U-1)^2=0. \tag{44}$$

In Eq. (44), $\cos\gamma$ appears in the form of

$$C\gamma = \frac{L_s}{M}\cos\gamma . \tag{45}$$

It can also be noted by examining Eqs. (41) and (42) that $\cos\gamma$ comes into the picture, as far as the study of the dynamics is concerned, always through the bias of S (or U) in Eq. (44). Therefore, it seems convenient to consider the firing-angle always in the form of Eq. (45). This enables one to suppress in Eqs. (41) and (42) any term that is not one of the nondimensional coefficients as defined so far, including $C\gamma$ (except for the factorizing terms).

Actually, $C\gamma$ allows for additional compactness in the present analysis. Indeed, the operating slip varies greatly according to which firing-angle is chosen (Fig. 2), which may hinder easy comparison of the stability of two operating points or two machines. However, the rotor frequency corresponding to a zero torque has been found to be [16]

$$\omega_{s\,T=o}^2 = \frac{R_s^2+L_s^2\omega_o^2}{M^2}\cos^2\gamma . \tag{46}$$

Authorized licensed use limited to: Missouri University of Science and Technology. Downloaded on July 17,2023 at 13:33:30 UTC from IEEE Xplore. Restrictions apply.

Expressed in a dimensionless form, this is

$$\tilde{\omega}_{s\,T=o}^{2} = (\sigma^2\alpha^2+\tilde{\omega}_o^2)\left(\frac{L_s}{M}\cos\gamma\right)^2 = C\gamma^2(\sigma^2\alpha^2+\tilde{\omega}_o^2). \qquad (47)$$

If the operating rotor frequency, $\tilde{\omega}_{so}$, is expressed with respect to $\tilde{\omega}_{sT=o}$, Eq. (47) indicates that it will be possible to link $\tilde{\omega}_{so}$ to simple parameters and have relatively simple analysis and comparisons.

Finally, it is interesting to note that many of the terms factorizing the numerator and the denominator cancel out, and their ratio reduces to

$$\frac{T_o}{\tilde{\omega}_{so}\alpha_r} = \frac{T_o}{\omega_{so}} \cdot \qquad (48)$$

Once associated with the inertia transfer function, this ratio forms in Eq. (38) the closed-loop gain, $\tilde{K}$, as follows:

$$\tilde{K} = \frac{nT_o}{J\tilde{\omega}_{so}\alpha_r^2} \cdot \qquad (49)$$

It can be noted that the gain, $\tilde{K}$, as expressed in Eq. (49) is the same as the one emerging from the study of the short-circuited case [14].

In conclusion, Table 2 completes Table 1 in collecting the parameters examined so far. They are enough to encompass all the different actual parameters of the machine, and the study of the root loci will be made with respect to them.

Table 2

New Nondimensional Parameters

$\alpha_r = (R_r+\frac{\pi^2}{18}R_F)/\sigma L_r$	New definition
$L_{DL} = \frac{\pi^2}{18}\frac{L_F}{\sigma L_r}$	Filter inductance parameter
$C_\gamma = \frac{L_s}{M}\cos\gamma$	Firing-angle parameter
$\tilde{K} = \frac{nT_o}{J\tilde{\omega}_{so}\alpha_r^2}$	Closed-loop gain

ROOT LOCI

For a given set of dimensionless parameters, the roots can be plotted, and the variation of $\tilde{K}$ (closed-loop gain) from zero to infinity will generate the root loci. The loci for typical parameters is presented first, after which the influence of each parameter is studied by comparison. Actually, these are very similar to the squirrel-cage loci [14].

General Form of the Root Loci

The basic form of the root loci is shown in Figure 4. It includes a branch that starts from the real axis. This moves up and eventually reaches instability before it crosses back to the end zero, the imaginary part of which actually corresponds approximately to $\tilde{\omega}_o$. It should be noted that the portion of the branch between the real axis and this accumulation area (including unstable points) corresponds to a small range of values of $\tilde{K}$. Moreover, this range of values depends greatly on the different parameters. The other branch starts from a nearby point and finally follows an asymptote, which is vertical when there is no filter inductance.

These plots must be completed by considering the third root, necessarily real. This root is negative for smaller values of slip and becomes positive beyond the peak torque. Two more roots, with negative imaginary parts, are located symmetrically with respect to the real axis and are not represented.

The root loci do not change significantly when α or σ changes. Their influence is not considered here, and all the plots are computed for $\alpha = 1$ and $\sigma = 0.05$. Novotny and his coworkers [14,16] studied them in other settings, and many of their conclusions are still true in this case.

The values of the other parameters are given on each plot. As far as the slip is concerned, it must be compared with the no-load slip (noted $s_{T=o}$), and both are written on each plot. In fact, $s - s_{T=o}$ is the entity which allows the comparison of different curves.

Influence of the Slip

For a given normalized stator frequency, $\tilde{\omega}_o$, the slip, s, is associated with the normalized rotor current frequency, $\tilde{\omega}_{so}$, as follows:

$$\tilde{\omega}_{so} = s\,\tilde{\omega}_o. \qquad (50)$$

As the slip (or $\tilde{\omega}_{so}$) increases, the values of $\tilde{K}$ that may lead to instability are larger. While the final and initial points remain at the same location, the lower branch tends to move upward and finally meets the upper branch. A new configuration then occurs (Fig. 5a) where the two former branches form a somewhat vertical locus, while the other roots form a loop close to the imaginary axis (slow mode).

For values of slip close to no-load slip, the magnitude of the third, real root is very large. It can be approximated by

$$\lambda = -U = -\frac{M\tilde{\omega}_{so}}{\sigma L_r}\frac{i_{soq}}{i_{ro}}, \qquad (51)$$

and, indeed, the steady-state torque and rotor current become zero together, explaining the large magnitude of λ. This root depends very little on $\tilde{K}$.

When $\tilde{K}$ is equal to zero, there is always a root at the origin (inertia pole), and it is provided at low slips by the lowest part of one of the two branches that includes part of the real axis (Figs. 4 and 5a).

For higher slips, however, this situation reverses. The real root starts from zero and moves on the real axis toward the value of $\lambda = -U$ but does not reach it. At the same time, none of the two other roots are purely real anymore (Fig. 5b). As for the values of slip of practical use, this configuration occurs only in special cases, for example when $\tilde{\omega}_o$ is small or γ is large.

Authorized licensed use limited to: Missouri University of Science and Technology. Downloaded on July 17,2023 at 13:33:30 UTC from IEEE Xplore. Restrictions apply.

Influence of the Firing-Angle

Figure 6a represents the roots for γ = 90 degrees, which in fact is the short circuited rotor case. Figure 4 corresponds to γ = 120 degrees, and Figure 6b to γ = 140 degrees. All three are for the same "relative" slip, $s - s_{T=o}$. The lower branch in the short-circuited case features a wider loop, which shrinks as γ becomes larger, leading eventually to the configuration with a vertical branch and a loop close to the imaginary axis (Fig. 6b). The unstable values of $\tilde{K}$ decrease as γ becomes larger.

Influence of the Normalized Frequency, $\tilde{\omega}_o$

Figure 7a represents a low normalized frequency ($\tilde{\omega}_o$=2) and Figure 7b a large value ($\tilde{\omega}_o$=16).

The final point of the lower branch ($\tilde{K}$=∞) and the initial point of the upper one ($\tilde{K}$=o) always have nearly the same imaginary parts. Their values are very close to $\tilde{\omega}_o$. Therefore, changes in $\tilde{\omega}_o$ indicate a stretching of the loci along the imaginary axis.

The sensitivity on the slip, as it has been explained, is greater for smaller normalized frequencies. For $\tilde{\omega}_o$=2, the small loop representing a slow mode for all values of $\tilde{K}$ appears even at a slip close to no-load, making such operations somewhat unstable.

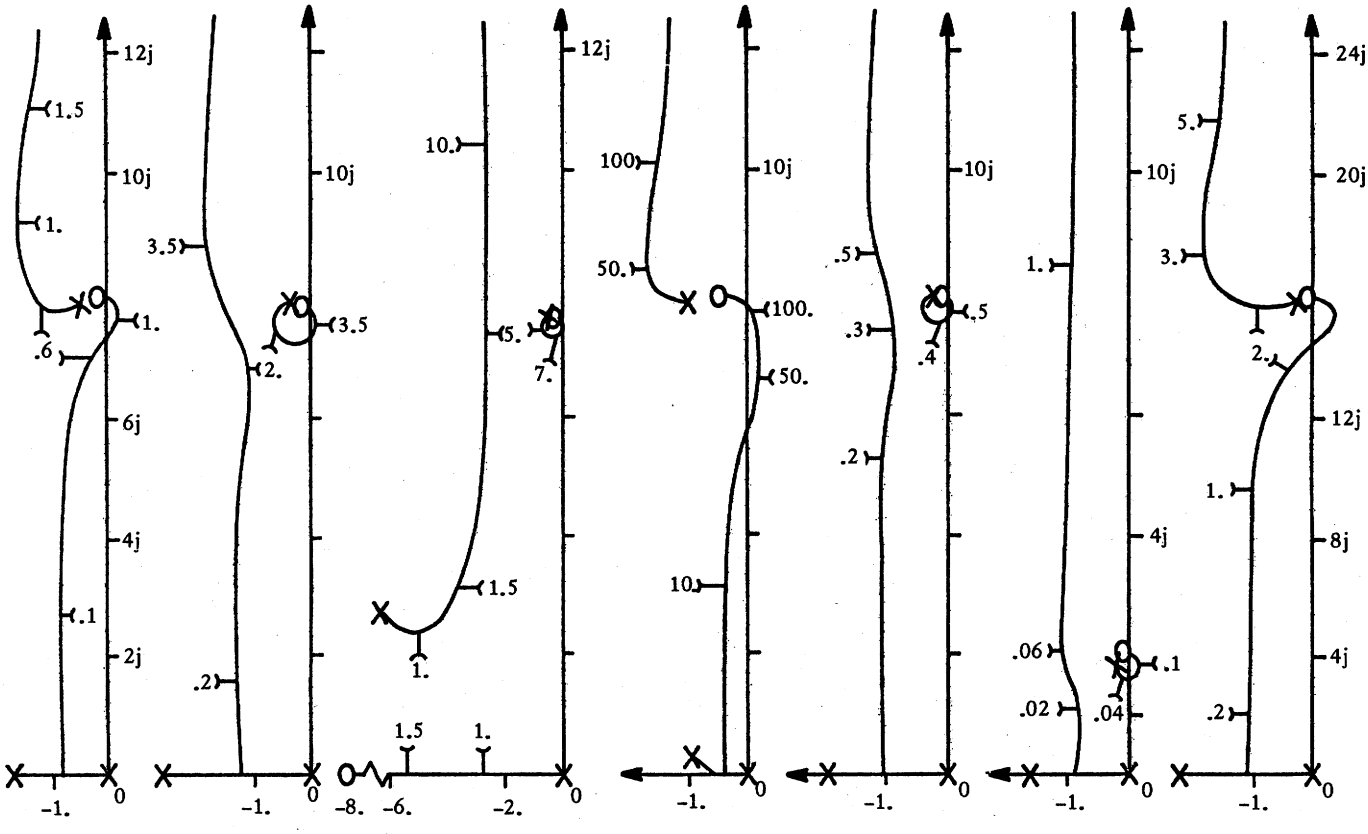

Fig. 4 Fig. 5a Fig. 5b Fig. 6a Fig. 6b Fig. 7a Fig. 7b

Fig. 4. Basic configuration: $\tilde{\omega}_o$ = 8, C_γ = -0.5, s = 0.51, $s_{T=o}$ = 0.50.

Fig. 5. Influence of slip s: $\tilde{\omega}_o$ = 8, C_γ = -0.5, (a) s = 0.55, $s_{T=o}$ = 0.50; (b) s = 0.65, $s_{T=o}$ = 0.50.

Fig. 6. Influence of firing-angle γ: $\tilde{\omega}_o$ = 8, (a) C_γ = 0, s = 0.01, $s_{T=o}$ = 0.0; (b) C_γ = -0.766, s = 0.776, $s_{T=o}$ = 0.766.

Fig. 7. Influence of normalized frequency $\tilde{\omega}_o$: C_γ = -0.5, s = 0.51, $s_{T=o}$ = 0.50; (a) $\tilde{\omega}_o$ = 2; (b) $\tilde{\omega}_o$ = 16.

Notes: Different points on the curves correspond to different values of $\tilde{K}$, some of which are on the plots. The same scale is always used except for Fig. 5b (real axis), and Fig. 7b (imaginary axis). All curves are drawn for α = 1, σ = 0.05, and L_F = 0.

Authorized licensed use limited to: Missouri University of Science and Technology. Downloaded on July 17,2023 at 13:33:30 UTC from IEEE Xplore. Restrictions apply.

Influence of the Filter Inductance

An idea of the evolution of the locus with respect to the filter inductance is given on Figure 8. Two curves are drawn, one for $L_F = 0$, the other one for $L_F \approx 0.9\, L_r$ (i.e., $L_{DL} = 10$). The basic configuration is the same, but the presence of the inductance produces a concentration of the complex roots around the imaginary axis. In other words, the inductance is slowing down the rate of decay of the transients.

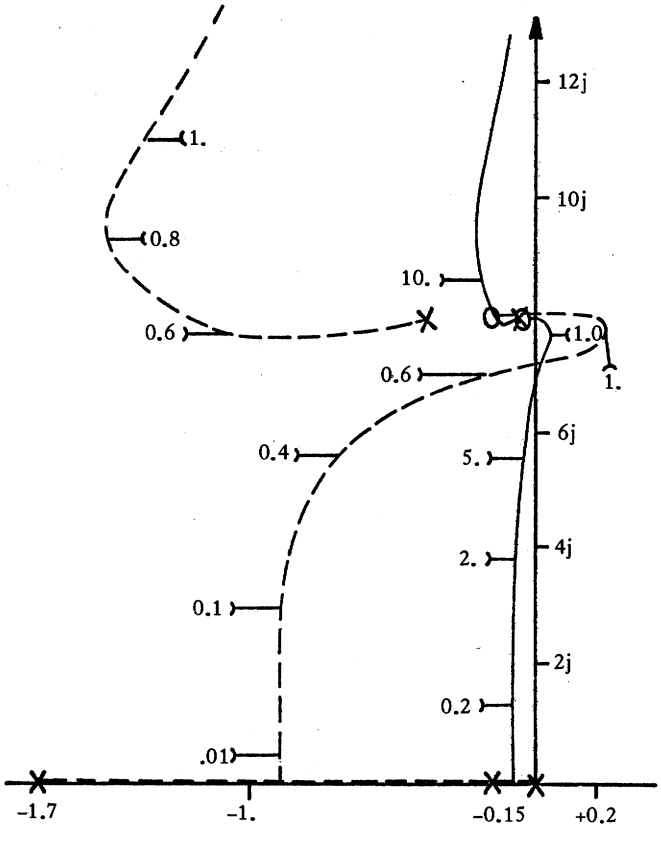

Fig. 8. Influence of the filter inductance. Both curves drawn for α=1, σ=0.05, $\tilde{\omega}_o = 8$, $C_\gamma = -0.5$, s=0.51, $s_{T=0}$ = 0.50. Dotted line: no filter inductance. Solid line: $L_{DL} = 10 <=> L_F \approx 0.9 L_r$.

USE OF THE LOCI

The use of the general loci can be illustrated by means of an example taken from the work of Mittle et al. [10].

Static Scherbius Drive

5 HP, 400 V, 4 pole, 50 Hz motor

Steady-state torque: 10.96 N.m

Steady-state slip: 0.4039

Firing angle: $\gamma = 110^o$

$R_s = 2.49\ \Omega$; $R_r = 3.09\ \Omega$; $R_F = o$; $L_F = o$

$L_s = 0.4096$ H; $L_r = 0.4096$ H; M = 0.3960 H

H = 0.075 s, (J = 0.0227 kg.m^2)

The following are computed:

$$\alpha = \frac{(2.49)(0.4096)}{(3.09)(0.4096)} = 0.81$$

$$\sigma = 1 - \frac{(0.3960)^2}{(0.4096)(0.4096)} = 0.0655$$

$$\alpha_r = \frac{3.09}{(0.0655)(0.4096)} = 115\ s^{-1}$$

$$\tilde{\omega}_o = \frac{314}{115} = 2.73;\ \tilde{\omega}_{so} = \frac{127}{115} = 1.10$$

$$\tilde{K} = \frac{2}{115(0.0227)}\ \frac{10.96}{127} = 0.0661$$

The normalized eigenvalues for shaft speed disturbances are taken from Figure 9. These are:

$-0.8 \pm j\,0.4$

$-0.23 \pm j\,2.5$

$-11.$

These are denormalized by being multiplied by α_r, to obtain:

$-92 \pm j\,46$	rad/s
$-26 \pm j\,287$	rad/s
-1265	rad/s

If a designer wishes to see what effect a doubling of rotor resistance has, for example, he just recomputes the new α, α_r, $\tilde{\omega}_o$, T_o, and $\tilde{\omega}_{so}$ values and proceeds in a similar manner. Several designs can be evaluated in a matter of minutes.

$\tilde{\omega}_o = 2.73$
$\alpha = 0.806$
$\sigma = 0.066$
$C_\gamma = -0.354$
$\gamma = 110^o$
$L_F = 0$
$s = 0.4039$
$s_{T=o} = 0.3539$

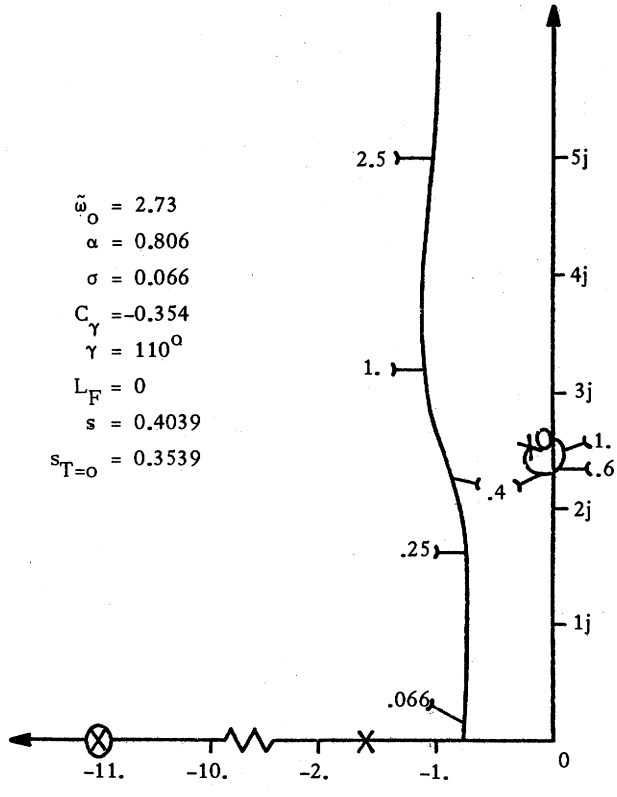

Fig. 9. The general loci for the cited example.

Authorized licensed use limited to: Missouri University of Science and Technology. Downloaded on July 17,2023 at 13:33:30 UTC from IEEE Xplore. Restrictions apply.

A stability analysis can be conducted, and in order to see the connection between the general loci and the stability boundaries in Mittle et al. [10], the torque for crossover into the right-hand plane is computed from the corresponding $\tilde{K}$ value of 0.6, in Fig. 8, using the $\tilde{K}$ equation in Table 2. This is done for several firing angles (figures similar to Fig. 9, but not included here). If the crossover $\tilde{K}$ values are attainable physically, we can compute the stability boundaries as given in [10] by plotting these torques versus firing angle.

CONCLUSIONS

The set of existing generalized root loci has been extended to include the static Scherbius machine in the subsynchronous mode. It was determined that these new loci are similar to those of the squirrel-cage machine and allow design options to be quickly evaluated without the computer.

It is fitting to mention, in addition, that these results do not necessarily imply more precision than previously used models. The main thrust of the paper is on the generalized nature of the results obtained.

The open-loop case was evaluated, and work is now underway to consider closed-loop configurations.

ACKNOWLEDGMENTS

Summer research salary support from the Graduate Office and the Engineering School of the University of Missouri-Rolla is greatfully acknowledged as well as that provided by the Power Group, Electrical Engineering Department, of the same University.

REFERENCES

1) C. P. Lemone and T. Takeushi, "Large Adjustable Speed Drives." IEEE, Power Engineering Society Summer Meeting, Paper 81SM416-7, 1981.

2) A. Lavi and R. J. Polge, "Induction Motor Speed Control with Static Inverter in the Rotor." IEEE Transactions on Power Apparatus and Systems, vol. PAS-85, no. 1.

3) P. N. Miljanic, "The Through-Pass Inverter and Its Application to the Speed Control of Wound Rotor Induction Machines." IEEE Transactions on Power Apparatus and Systems, vol. PAS-87, no. 1, pp. 234-239, 1968.

4) W. Shepherd and J. Stanway, "Slip Power Recovery in an Induction Motor by the Use of a Thyristor Inverter." IEEE Transactions on Industry and General Applications, vol. IGA-5, no. 1, pp. 74-82, 1969.

5) B. M. Bird and P. Mehta, "Regenerative Braking in Slip-Power-Recovery Systems." Proceedings IEEE, vol. 119, no. 9, pp. 1343-1344, 1972.

6) G. A. Smith, "Static Scherbius System of Induction-Motor Speed Control." Proceedings IEEE, vol. 124, no. 6, pp. 557-560, 1977.

7) V. Pavlov, H. Okitsu, T. Suzuki, and T. Ohnishi, "Hybrid Speed-Control System of Wound-Rotor Induction Motor." Proceedings IEE , vol. 126, no. 9, pp. 821-825, 1979.

8) G. Giannakopoulos and S. Galanos, "Dynamic Simulation of an Induction Motor Drive with D. C. Link in the Rotor Circuits." IEEE, Power Engineering Society Winter Meeting, Paper A79112-4, 1979.

9) V. N. Mittle, K. Venkatesan, and S. C. Gupta, "Switching Transients in Static Slip-Energy Recovery Drive." IEEE Transactions on Power Apparatus and Systems, vol. PAS-98, no. 4, pp. 1315-1320, 1979.

10) V. N. Mittle, K. Venkatesan, and S. C. Gupta, "Stability Analysis of a Constant Torque Static Slip-Power-Recovery Drive." IEEE, Transactions on Industry Applications, vol. IA-16, no. 1, pp. 119-126, 1980.

11) T. Tsuchiya, "Suboptimal Control of a Static Scherbius Induction Motor System Using a Microprocessor." IEEE Transactions on Industry Applications, vol. IA-16, no. 5, pp. 686-699, 1980.

12) P. Franz and A. Meyer, "Digital Simulation of a Complete Subsynchronous Converter Cascade with 6/12-Pulse Feedback System." IEEE Transactions on Power Apparatus and Systems, vol. PAS-100, no. 12, pp. 4948-4957, 1981.

13) G. A. Smith, "A Current-Source Inverter in the Secondary Circuit of a Wound Rotor Induction Motor Provides Sub- and Supersynchronous Operation." IEEE Transactions on Industry Applications, vol. IA-17, no. 4, pp. 399-406, 1981.

14) D. W. Novotny and J. H. Wouterse, "Induction Machine Transfer Functions and Dynamic Response by Means of Complex Time Variables." IEEE Transactions on Power Apparatus and Systems, vol. PAS-95, no. 4, pp. 1325-1335, 1976.

15) R. Stern and D. W. Novotny, "A Simplified Approach to the Determination of Induction Machine Dynamic Response." IEEE Transactions on Power Apparatus and Systems, vol. PAS-97, no. 4, pp. 1430-1439, 1978.

16) A. R. Miles and D. W. Novotny, "Transfer Functions of the Slip-Controlled Induction Machine." IEEE Transactions on Industry Applications, vol. IA-15, no. 1, pp. 54-62, 1979.

17) M. Abbas and D. W. Novotny, "The Stator Voltage-Controlled Current Source Inverter Induction Motor Drive." IEEE Transactions on Industry Applications, vol. IA-18, no. 3, pp. 219-230, 1982.

Authorized licensed use limited to: Missouri University of Science and Technology. Downloaded on July 17,2023 at 13:33:30 UTC from IEEE Xplore. Restrictions apply.

APPENDIX A: DEFINITIONS AND SYMBOLS

The machine inpedances are defined in a d-q axis frame under their operational form as follows:

$$Z_s = R_s + L_s p + jL_s \omega$$

$$Z_m = Mp + jM\omega$$

$$Z_r = R_r + L_r p + jL_r \omega_s$$

$$Z_d = Mp + jM\omega_s$$

The terms in p vanish when steady-state values are considered.

Notations

i	a.c. currents
I_R	direct current (see Fig. 1)
J	inertia
L	self-inductances
M	mutual inductances
n	number of pairs of poles
R	resistances
s	slip
T	electric torque
T_L	mechanical torque
v	a.c. voltages
V_I, V_R	direct voltages (see Fig. 1)
Z	complex impedances (see above)
ω	stator current frequency
ω_r	electric rotor velocity
ω_s	rotor current frequency

Subscripts

d	direct axis
q	quadratic axis
r	rotor
s	stator
o	steady-state
F	filter parameters (see Fig. 1)

Also, $\sim$ on a symbol denotes its normalized value. Re(z), Im(z), and z* denote respectively the real part, imaginary part, and conjugate of the complex entity z.

Authorized licensed use limited to: Missouri University of Science and Technology. Downloaded on July 17,2023 at 13:33:30 UTC from IEEE Xplore. Restrictions apply.